Scilight

Intelligence & Control
https://www.sciltp.com/journals/ic

Article

Filter-Based Adaptive Fuzzy Control for an Uncertain Robotic Manipulator with Intermittent Input and Output Triggering

Jihang Sui [1], Alain Martinez [2], Ben Niu [3,*], Yunfei Mu [4,5], Deepak Kumar Jain [3] and Dmytro Zubov [6]

[1] School of Information Science and Engineering, Shandong Normal University, Jinan 250014, China
[2] Department of Automatic Control, Marta Abreu Central University of Las Villas, Santa Clara 50100, Cuba
[3] Key Laboratory of Intelligent Control and Optimization for Industrial Equipment of Ministry of Education, School of Control Science and Engineering, Dalian University of Technology, Dalian 116024, China
[4] State Key Laboratory of Synthetical Automation for Process Industries and the College of Information Science and Engineering, Northeastern University, Shenyang 110004, China
[5] Foshan Graduate School of Innovation, Northeastern University, Foshan 528311, China
[6] Department of Computer Science, University of Central Asia, Naryn 722900, Kyrgyzstan
* Correspondence: niuben@dlut.edu.cn

How To Cite: Sui, J.; Martinez, A.; Niu, B; et al. Filter-Based Adaptive Fuzzy Control for an Uncertain Robotic Manipulator with Intermittent Input and Output Triggering. *Intelligence & Control* **2025**, *1*(1), 5. https://doi.org/10.53941/ic.2025.100005

Received: 12 Novermber 2025
Revised: 3 December 2025
Accepted: 17 December 2025
Published: 24 December 2025

Abstract: This paper investigates the adaptive output feedback control issue for an uncertain robotic manipulator (RM) under input and output triggering. Due to the influence of the output-triggering mechanism, the output state becomes discrete, thereby leading to the non-differentiability problem of the virtual controller. Therefore, a first-order low-pass filter is constructed to generate a filtered version of the sampled output with continuous differentiability for controller design. By utilizing the fuzzy logic systems (FLSs), the unknown robotic dynamics are effectively approximated without requiring the global Lipschitz condition. Subsequently, an adaptive fuzzy state observer is developed based on the filtered output signal to estimate the joint velocity of the RM. Based on the Lyapunov stability analysis method of the hybrid system, it is rigorously proved that all signals of the RM are bounded, and Zeno behavior is precluded. Furthermore, the designed event-triggered control protocol can ensure the desirable system performance and reduce communication resources even under output discretization. Finally, a two-link RM is employed to verify the effectiveness of the control protocol.

Keywords: uncertain robotic manipulator; event-triggered control; adaptive filtering method; fuzzy logic systems; output feedback control

1. Introduction

Because robotic manipulators (RMs) exhibit strong nonlinearity and high coupling characteristics, their control problems have long been an important research topic in the field of automation. Moreover, RMs have been widely applied in various fields such as industrial manufacturing [1,2], military [3,4], and medical care [5,6]. Therefore, numerous researchers have conducted extensive and in-depth studies on the control methods of RMs. For example, ref. [7] proposed an adaptive control strategy based on the forward stepping approach for the RM with closed architecture. In [8], the sliding mode control method was developed to achieve trajectory tracking for the industrial RM system. However, due to the high cost and susceptibility to noise interference of speed sensors, the speed information is often difficult to measure directly, which makes all the above methods have significant limitations in practical applications. In response to this issue, many studies [9–13] have developed the observer-based output feedback control methods to estimate the system states under unmeasurable velocity conditions, thereby ensuring

satisfactory control performance. Note that the above works all adopt continuous-time control strategies. With the widespread application of communication networks in control systems, the traditional continuous-time control and periodic sampling methods generate a large volume of redundant data due to frequent signal updates, thereby wasting limited network bandwidth.

To save communication resources, the event-triggered control (ETC) methods [14–19] have been proposed. Such control methods determine when to update control signals by setting triggering conditions, thereby significantly reducing the number of transmissions. The ETC strategy with a dynamic event-triggered mechanism (ETM) was proposed in [14] to solve the tracking control issue of the RM. Ref. [15] proposed the output feedback controller based on the switching ETM for the nonlinear interconnected system. It is worth noting that the above works only focus on the resource utilization in the controller-to-actuator channel. The information from the sensor-to-controller channel is still continuously transmitted, and the control input is calculated based on continuous state variables. In practical applications, RMs are often deployed in resource constrained scenarios, such as mobile platforms [20] or remote operating systems [21]. Due to limited battery power and communication bandwidth, continuous communication from the sensor to the controller is difficult to achieve. Especially when the system state changes rapidly, frequent transmissions not only waste resources but may also cause problems such as redundant control, transmission delays, and network congestion. Therefore, from the perspective of saving communication resources, the ETM transmits data only when there is a significant change in the system state. This not only helps to reduce the system burden but also improves resource utilization while ensuring control performance. Thus, introducing the ETM on the sensor-to-controller channel has important practical significance.

Based on the above analysis, many state-triggering and output-triggering control strategies have been proposed by scholars [22–26]. To achieve the trajectory tracking of the surface vessel, the model-based state-triggering control method was developed in [22]. Based on event-sampling states, ref. [23] proposed the adaptive fuzzy ETC scheme for the nonlinear multi-agent systems. However, the works in [22,23] failed to solve the problem of non-differentiability in virtual controllers. Due to the introduction of the ETM into the sensor-to-controller channel, state variables become discontinuous sampled values, resulting in the virtual controllers no longer being continuous. Traditional backstepping methods cannot calculate their derivatives, which may cause unacceptable jumps at the triggered moments. To address this issue, ref. [24–26] introduced the dynamic surface control (DSC) methods to avoid taking derivatives of virtual controllers. Although considerable progress has been made in the design of differentiable virtual controllers, these methods are limited to systems whose functions satisfy global Lipschitz conditions or whose unknown parameters are restricted to known compact sets, rendering them unsuitable for direct application to the RM system.

By using the dual asynchronous ETMs of the system output and the control input, this paper designs an adaptive ETC scheme for an uncertain RM system, which does not require continuous data transmission throughout the entire control process. The contributions of this paper are summarized as follows:

(i) Regarding the existing ETC strategies [14–17] that do not consider the resource consumption issue in the sensor-to-controller channel, this paper designs the dual asynchronous ETMs combining the system output and the control input, thereby further saving communication resources. Moreover, compared with the methods in [24,27,28], the proposed control scheme reduces the number of ETMs and communication channels, further lowering the computational and communication burdens of the system.

(ii) In this paper, a low-pass filter is constructed to take the sampled output as input and generate a necessarily differentiable filtered variable for controller design. Based on this, under the DSC framework, the filtered variable is employed to design the differentiable virtual controller, effectively avoiding the design difficulties caused by the non-differentiability of traditional virtual controllers [22,23].

(iii) FLSs are utilized to approximate the unknown nonlinear dynamics of the RM and integrated into the state observer to enable estimation of the unmeasurable joint velocity. Compared to the assumption in [24,26,27] that the nonlinear term must satisfy the global Lipschitz condition, this paper relaxes this requirement, thereby expanding the applicability of the control method. In addition, based on the stability lemma of the hybrid system, the boundedness of all signals in the RM is rigorously proved.

Notation 1. *In this paper,* $\mathbb{N}$, $\mathbb{R}^n$, *and* $\mathbb{R}^{n\times m}$ *denote the set of natural numbers, the* n*-dimensional real vector space, and the set of* $n \times m$ *real matrices, respectively.* $diag\{\gamma_1 \ldots, \gamma_n\}$ *is the diagonal matrix, and* $\|x\|$ *stands for the Euclidean norm of the vector* $x \in \mathbb{R}^n$. *The symbols* $\mathbf{I}$ *and* $\mathbf{0}$ *represent the identity matrix and the zero vector (matrix) with appropriate dimensions, respectively. The minimum and maximum eigenvalues of a matrix are denoted by* $\lambda_{\min}(\cdot)$ *and* $\lambda_{\max}(\cdot)$. *Besides,* $\upsilon(t^+) = \lim_{a\to 0^+}\upsilon(t+a)$ *and* $\Delta\upsilon(t) = \upsilon(t^+) - \upsilon(t)$ *are defined.*

2. Problem Statement and Preliminaries

The n-link uncertain rigid RM dynamic equation is described as follows:

$$\begin{aligned} M_0(q)\ddot{q}+&C_0(q,\dot{q})\dot{q}+G_0(q)+\Delta N(q,\dot{q},\ddot{q}) \\ &+\gamma(t-T_f)\varphi(q,\dot{q})=\tau, \end{aligned} \tag{1}$$

where q, $\dot{q}$, $\ddot{q}\in\mathbb{R}^n$ are the joint position, velocity, and acceleration vectors, respectively. $M_0(q)\in\mathbb{R}^{n\times n}$, $C_0(q,\dot{q})\in\mathbb{R}^{n\times n}$ and $G_0(q)\in\mathbb{R}^n$ denote the nominal values of the inertia matrix, Coriolis and centripetal matrix, and gravity vector, respectively. $\tau\in\mathbb{R}^n$ is the torque input. $\varphi(q,\dot{q})$ represents the process fault component in the RM. $\gamma(t-T_f)$ is the time curve of the fault, where T_f is the time when the fault occurs. $\Delta N(q,\dot{q},\ddot{q})$ stands for the uncertain dynamics of the RM, which arise from the uncertain matrices $\Delta M(q)$, $\Delta C(q,\dot{q})$, $\Delta G(q)$, and the friction vector $F(q,\dot{q})\in\mathbb{R}^n$. $\Delta N(q,\dot{q},\ddot{q})$ can be formulated as

$$\Delta N(q,\dot{q},\ddot{q})=\Delta M(q)\ddot{q}+\Delta C(q,\dot{q})\dot{q}+\Delta G(q)+F(q,\dot{q}). \tag{2}$$

The matrix $\gamma(t-T_f)$ is given by

$$\gamma(t-T_f)=diag\{\gamma_1(t-T_f),\ldots,\gamma_n(t-T_f)\}, \tag{3}$$

where $\gamma_i(\cdot)$ is defined as follows:

$$\gamma_i(t-T_f)=\begin{cases}0, & t<T_f\\ 1-e^{-\ell_i(t-T_f)}, & t\geq T_f\end{cases} \tag{4}$$

where $\ell_i>0$ denotes the development of the fault. If ℓ_i is small, the initial fault is postulated. In contrast, if ℓ_i is large, the abrupt fault exists.

Property 1. *[29]: The matrix $M_0(q)$ is symmetric positive definite and bounded, with its bound denoted by $\partial_a<\|M_0(q)\|<\partial_b$, where ∂_a and ∂_b are positive constants.*

Property 2. *[29]: There exist positive constants ∂_c, ∂_d, and ∂_e such that $\partial_c<\left\|M_0^{-1}(q)\right\|<\partial_d$ and $\|G_0(q)\|\leq\partial_e<\infty$.*

Lemma 1. *[30]: By exploiting the universal approximation capability of the FLS, we have*

$$f(x)=W^TS(x)+\varepsilon(x),\quad \forall x\in\Omega_x, \tag{5}$$

where $f(x)$ denotes an unknown nonlinear function vector, and $W=[W_1(x),\ldots,W_l(x)]^T\in\mathbb{R}^{l\times n}$ is the weight matrix. The vector $S(x)=[S_1(x),\ldots,S_l(x)]^T\in\mathbb{R}^l$ stands for the fuzzy basis function, satisfying $0<S^T(x)S(x)\leq 1$, and l is the number of fuzzy rules. The approximation error $\varepsilon(x)$ is bounded by $\|\varepsilon(x)\|\leq\bar{\varepsilon}$, where $\bar{\varepsilon}$ is an unknown constant.

Now, let $x_1=q=[x_{1,1},\ldots,x_{1,n}]^T$ and $x_2=\dot{q}$, the system (1) is rewritten in the following form:

$$\begin{cases}\dot{x}_1=x_2,\\ \dot{x}_2=\Gamma\tau+f(x)=\Gamma\tau+W^TS(x)+\varepsilon(x),\end{cases} \tag{6}$$

where $f(x)=M_0^{-1}(x_1)[-C_0(x_1,x_2)x_2-G_0(x_1)-\Delta N(x_1,x_2,\dot{x}_2)-\gamma(t-T_f)\varphi(x_1,x_2)]$ represents the uncertain term, $x=[x_1^T,x_2^T]^T\in\mathbb{R}^{2n}$, and $\Gamma=M_0^{-1}(x_1)$.

3. Event-Triggered Control of Robotic Manipulator System

3.1. Dual Event-Triggered Mechanisms

To maximize the conservation of communication resources, this paper designs the ETMs separately on the sensor-to-controller and controller-to-actuator channels, thereby ensuring good tracking performance while reducing communication frequency. The output ETM is designed as follows:

$$t_{x,i}^{m+1}=\inf\{t>t_{x,i}^m:|x_{1,i}(t)-\breve{x}_{1,i}(t)|\geq\delta_{x1}\}$$

$$\breve{x}_{1,i}(t) = x_{1,i}(t_{x,i}^m), \quad \forall t \in [t_{x,i}^m, t_{x,i}^{m+1}) \tag{7}$$

where $i = 1, 2, \ldots, n$, $m \in \mathbb{N}$, and $t_{x,i}^m$ denotes the triggering instant for the sensor output with $t_{x,i}^0 = 0$. δ_{x1} is the positive constant. $\breve{x}_{1,i}$ represents the sampled value of $x_{1,i}$ at $t_{x,i}^m$, and it remains unchanged during the interval $t \in [t_{x,i}^m, t_{x,i}^{m+1})$.

The following control input ETM is constructed:

$$\begin{aligned} t_{\tau,i}^{\bar{m}+1} &= \inf\{t > t_{\tau,i}^{\bar{m}} : |u_i(t) - \tau_i(t)| \geq \delta_\tau\} \\ \tau_i(t) &= u_i(t_{\tau i}^{\bar{m}}), \quad \forall t \in [t_{\tau,i}^{\bar{m}}, t_{\tau,i}^{\bar{m}+1}) \end{aligned} \tag{8}$$

where $\bar{m} \in \mathbb{N}$, and $t_{\tau,i}^{\bar{m}}$ is the input triggering instant with $t_{\tau,i}^0 = 0$. $\delta_\tau > 0$ denotes the triggering threshold, and the control input u_i will be designed later in (20).

To solve the issue of virtual controllers being non-differentiable due to the instantaneous jump of $\breve{x}_{1,i}$ at time $t_{x,i}^m$, the following first-order filter is introduced:

$$\eta_1 \dot{x}_{1f,i} + x_{1f,i} = \breve{x}_{1,i}, \quad \forall t \in [t_{x,i}^m, t_{x,i}^{m+1}) \tag{9}$$

where $\eta_1 > 0$ is the filter gain, and $x_{1f,i}$ is the filtered version of $\breve{x}_{1,i}$.

Remark 1. *In the general backstepping design framework, the differentiation of virtual controllers relies on the derivatives of state variables. However, under the output ETM, only the sampled output $\breve{x}_1$ is available, which renders the constructed virtual controller non-differentiable and thus hinders the direct application of the recursive backstepping method. To overcome the above challenge, this paper designs the filter (9) to generate the continuously differentiable variable x_{1f} to replace $\breve{x}_1$.*

3.2. Fuzzy State Observer Design

Since only the state x_1 is measurable, an adaptive fuzzy state observer is designed based on the filtered sampled output x_{1f} to estimate the unmeasurable state vector as follows:

$$\begin{cases} \dot{\hat{x}}_1 = \hat{x}_2 + K_1(x_{1f} - \hat{x}_1), \\ \dot{\hat{x}}_2 = \Gamma\tau + \hat{W}^T S(\hat{x}) + K_2(x_{1f} - \hat{x}_1), \end{cases} \tag{10}$$

where $\hat{x}_i = [\hat{x}_{i,1}, \ldots, \hat{x}_{i,n}]^T \in \mathbb{R}^n$ $(i = 1, 2)$ is the estimate of x_i. $K_1 = diag\{k_{1,1}, \ldots, k_{1,n}\}$ and $K_2 = diag\{k_{2,1}, \ldots, k_{2,n}\}$ are the observer gains. $\hat{W}$ denotes the weight estimate of W and $\hat{x} = [\hat{x}_1^T, \hat{x}_2^T]^T \in \mathbb{R}^{2n}$.

To facilitate the observer analysis and the controller design, the following error variables are defined: $e_i = x_i - \hat{x}_i (i = 1, 2)$ are the observer errors; $\tilde{W} = W - \hat{W}$ is the weight estimation error; $\pi_1 = x_{1f} - \breve{x}_1$ denotes the filter error; $\mu_1 = x_1 - \breve{x}_1$ is the measurement error.

It can be derived from (6) and (10) that

$$\begin{cases} \dot{e}_1 = -K_1 e_1 + e_2 - K_1(\pi_1 - \mu_1), \\ \dot{e}_2 = -K_2 e_1 - K_2(\pi_1 - \mu_1) + \tilde{W}^T S(\hat{x}) + \theta(\hat{x}, x) + \varepsilon(x), \end{cases} \tag{11}$$

where $\theta(\hat{x}, x) = W^T S(x) - W^T S(\hat{x})$.

From (11), the derivative of $e = [e_1^T, e_2^T]^T \in \mathbb{R}^{2n}$ is given as follows:

$$\dot{e} = Ae + F - KB, \tag{12}$$

where

$$\begin{aligned} A &= \begin{bmatrix} -K_1 & \mathbf{I}_{n\times n} \\ -K_2 & \mathbf{0}_{n\times n} \end{bmatrix}, B = \begin{bmatrix} \pi_1 - \mu_1 \\ \pi_1 - \mu_1 \end{bmatrix}, \\ K &= \begin{bmatrix} K_1 & \mathbf{0}_{n\times n} \\ \mathbf{0}_{n\times n} & K_2 \end{bmatrix}, F = \begin{bmatrix} \mathbf{0}_{n\times 1} \\ F_1 \end{bmatrix}, \\ F_1 &= \tilde{W}^T S(\hat{x}) + \theta(\hat{x}, x) + \varepsilon(x). \end{aligned}$$

By appropriately choosing the gains K_1 and K_2, the matrix A is Hurwitz. Consequently, there exist the

symmetric positive definite matrices P and Q such that $A^TP + PA = -Q$.

Define the Lyapunov function as

$$V_e = e^TPe. \tag{13}$$

Taking the derivative of (13), one yields

$$\begin{aligned}\dot{V}_e =&2e^TP(Ae + F - KB)\\ \leq& - e^TQe + 2\|e\|\|P\|\|F\| + 2\|e\|\|P\|\|K\|\|B\|\\ \leq& - (\lambda_{\min}(Q) - 5)\|e\|^2 + \|P\|^2||\tilde{W}||^2\\ &+ 4\|P\|^2\|K\|^2\pi_1^T\pi_1 + \Xi,\end{aligned} \tag{14}$$

where $\Xi = 2\|P\|^2\|W\|^2 + \|P\|^2\bar{\varepsilon}^2 + 4n\|P\|^2\|K\|^2\delta_{x1}^2$. To derive (14), the inequalities $2\|e\|\|P\|\|K\|\|B\| \leq \|e\|^2 + 4\|P\|^2\|K\|^2\pi_1^T\pi_1 + 4n\|P\|^2\|K\|^2\delta_{x1}^2$ and $2\|e\|\|P\|\|F\| = 2\|e\|\|P\|\|F_1\| \leq 4\|e\|^2 + \|P\|^2||\tilde{W}||^2 + 2\|P\|^2\|W\|^2 + \|P\|^2\bar{\varepsilon}^2$ are used.

3.3. Adaptive Controller Design

In this section, the backstepping-based adaptive control method is proposed for the RM system (1). Under the framework of DSC, the following coordinate transformation is defined:

$$z_1 = \hat{x}_1, \tag{15}$$

$$z_2 = \hat{x}_2 - \omega_2, \tag{16}$$

$$\beta = \omega_2 - \alpha_1, \tag{17}$$

where z_1 and z_2 are the stabilizing errors. β denotes the boundary error. The signal ω_2 is generated by passing the virtual controller α_1 through the following filter to address the "explosion of complexity" issue encountered in the traditional backstepping method:

$$\xi\dot{\omega}_2 + \omega_2 = \alpha_1, \quad \omega_2(0) = \alpha_1(0), \tag{18}$$

where $\xi > 0$ is a design constant.

Then, the virtual controller α_1, the control input u_i and the adaptive law $\dot{\hat{W}}_i$ are designed as

$$\alpha_1 = - (c_1 + 0.5)z_1 - K_1(x_{1f} - \hat{x}_1), \tag{19}$$

$$\begin{aligned}u =&\Gamma^{-1}[-z_1 - (c_2 + 1)z_2 - \hat{W}^TS(\hat{x})\\ &- K_2(x_{1f} - \hat{x}_1) + \dot{\omega}_2],\end{aligned} \tag{20}$$

$$\dot{\hat{W}}_i = \Gamma_i(z_{2,i}S(\hat{x}) - \sigma_i\hat{W}_i), \quad i = 1, \ldots, n, \tag{21}$$

where c_1, c_2 and σ_i are the positive design constants. $\Gamma_i \in \mathbb{R}^{l\times l} > 0$ denotes a diagonal adjustment matrix.

Selecting the total Lyapunov function as

$$\begin{aligned}V =&V_e + V_{\pi 1} + V_{z1} + V_{z2} + V_\beta\\ =&e^TPe + \frac{1}{2}\pi_1^T\pi_1 + \frac{1}{2}z_1^Tz_1\\ &+ \left(\frac{1}{2}z_2^Tz_2 + \frac{1}{2}\sum_{i=1}^{n}\tilde{W}_i^T\Gamma_i^{-1}\tilde{W}_i\right) + \frac{1}{2}\beta^T\beta.\end{aligned} \tag{22}$$

Before conducting the stability analysis, it should be noted that due to the discontinuity of the sampled output $\breve{x}_1$ at the triggering instants, the closed-loop system involving the variable π_1 exhibits a jump set, rendering the traditional continuous-time Lyapunov stability analysis methods inapplicable. To address the above issue, this paper introduces the concept of a hybrid system model (see Definition 1), which is commonly used to analyze complex systems involving both continuous dynamics and discrete events. The model typically consists of two types of equations: (i) the differential equation that describes the system evolution over continuous time intervals; (ii) the difference equation that characterizes the system behavior at discrete triggering instants.

Definition 1. *[31]: The hybrid system $H(C, E_c(\upsilon), D, E_d(\upsilon))$ is represented as a quadruple, where $C \subset \mathbb{R}^n$ is the flow set, and the state $\upsilon \in \mathbb{R}^n$ evolves continuously within this set according to the differential equation $\dot{\upsilon} = E_c(\upsilon)$; $D \subset \mathbb{R}^n$ represents the jump set, where the state $\upsilon \in \mathbb{R}^n$ undergoes discrete updates via the differential inclusion $\Delta\upsilon(t) \in E_d(\upsilon)$. The vector fields $E_c(\upsilon) : \mathbb{R}^n \to \mathbb{R}^n$ and $E_d(\upsilon) : \mathbb{R}^n \Rightarrow \mathbb{R}^n$ correspond to the flow map and the set-valued map, respectively.*

Lemma 2. *[32]: If there is a function $V(\upsilon)$ such that the following relationships hold:*

$$\hbar_a(||\upsilon||) \leqslant V(\upsilon) \leqslant \hbar_b(||\upsilon||), \quad \upsilon \in \{C \cup D\} \tag{23}$$

$$\frac{\partial V(\upsilon)}{\partial \upsilon} E_c(\upsilon) < 0, \quad \upsilon \in C \tag{24}$$

$$\Delta V(\upsilon) \leqslant 0, \quad \upsilon \in D \tag{25}$$

where $\hbar(\cdot)$ is a class $\mathcal{K}_\infty$ function, then the nonlinear hybrid system is ultimately bounded.

Define $\upsilon = [\upsilon_1^T, \upsilon_2^T]^T \in \mathbb{R}^{(l+6)n}$ as the augmented error, with $\upsilon_1 = [z_1^T, e_1^T, \pi_1^T]^T \in \mathbb{R}^{3n}$ and $\upsilon_2 = [z_2^T, e_2^T, \beta^T, \tilde{W}_i^T]^T \in \mathbb{R}^{(l+3)n}$, $i = 1, \ldots, n$. Then, the hybrid system is defined as follows:

$$H(C, E_c(\upsilon), D, E_d(\upsilon)) = \begin{cases} \dot{\upsilon} = E_c(\upsilon), & \upsilon \in C \\ \Delta\upsilon = E_d(\upsilon), & \upsilon \in D \end{cases} \tag{26}$$

where $E_c(\upsilon) \in \mathbb{R}^{(l+6)n}$ and $E_d(\upsilon) \in \mathbb{R}^{(l+6)n}$ will be defined afterward.

Based on Lemma 1, the analysis of the system (26) is divided into the following two cases:

Case 1. *Define the flow set C as*

$$C = \left\{ \upsilon \in \mathbb{R}^{(l+6)n} \middle| |x_{1,i} - \breve{x}_{1,i}| < \delta_{x1} \right\}, \tag{27}$$

where the set C characterizes the dynamic behavior of the error υ within the time interval defined by the adjacent triggering instants $t_{x,i}^m$ and $t_{x,i}^{m+1}$, i.e., for all $t \in [t_{x,i}^m, t_{x,i}^{m+1})$.

The evolution of the augmented error is described by $\dot{\upsilon}_i = E_{c,i}(\upsilon_i)$ for $i = 1, 2$. The first n rows of $E_{c,i}(\upsilon_i)$ describe the evolution of stabilizing errors, which are derived as

$$\begin{cases} \dot{z}_1 = \hat{x}_2 + K_1(x_{1f} - \hat{x}_1), \\ \dot{z}_2 = \Gamma\tau + \hat{W}^T S(\hat{x}) + K_2(x_{1f} - \hat{x}_1) - \dot{\omega}_2. \end{cases} \tag{28}$$

The rows from $(n+1)$ to $2n$ describe the dynamics of the observer errors, as given in (11). The derivatives of π_1 and β, given by the rows $(2n+1)$ to $3n$, are expressed as follows:

$$\dot{\pi}_1 = \dot{x}_{1f} = -\pi_1/\eta_1, \tag{29}$$

$$\dot{\beta} = -\beta/\xi + \rho(\cdot), \tag{30}$$

where $\rho(\cdot) = -\dot{\alpha}_1$, and the value of $\breve{x}_1$ stays constant in the set C.

The last (nl) rows describe the dynamics of the weight estimation error $\tilde{W}_i$, based on (21), as follows:

$$\dot{\tilde{W}}_i = -\dot{\hat{W}}_i = -\Gamma_i(z_{2,i} S(\hat{x}) - \sigma_i \hat{W}_i). \tag{31}$$

Case 2. *The jump set D within the hybrid system (26) is characterized as*

$$D = \left\{ \upsilon \in \mathbb{R}^{(l+6)n} \middle| |x_{1,i} - \breve{x}_{1,i}| \geq \delta_{x1} \right\}, \tag{32}$$

where this set defines the jump map of the error υ at the triggering instants, for all $t = t_{x,i}^m$.

For $\forall t = t_{x,i}^m$, we can obtain

$$\begin{bmatrix} \upsilon_1(t^+) \\ \upsilon_2(t^+) \end{bmatrix} = \begin{bmatrix} [z_1^T(t), e_1^T(t), (x_{1f}(t) - \breve{x}_1(t^+))^T]^T \\ \upsilon_2(t) \end{bmatrix}. \tag{33}$$

As a result, one gets

$$\Delta\upsilon_1(t) = [\mathbf{0}_{n\times1}^T, \mathbf{0}_{n\times1}^T, (\breve{x}_1(t) - \breve{x}_1(t^+))^T]^T, \tag{34}$$

$$\Delta\upsilon_2(t) = [\mathbf{0}_{n\times1}^T, \mathbf{0}_{n\times1}^T, \mathbf{0}_{n\times1}^T, \mathbf{0}_i^T]^T, \quad i = 1, \ldots, n, \tag{35}$$

where the vector $\mathbf{0}_i$ is the l-dimensional zero column vector.

3.4. Stability Analysis

Theorem 1. *Consider the n-link uncertain RM (1) with the dual ETMs (7) and (8). The designed state observer (10), the virtual controller (19), the actual controller (20), and the adaptive law (21) can guarantee that all signals are uniformly bounded under bounded initial conditions, and Zeno behavior is precluded.*

Proof. To be consistent with the two cases in the controller design section, the stability analysis is also divided into Cases 1 and 2. □

In the Flow Set C (Case 1): The derivative of V_e has been provided in (14). Based on (29) and (30), $\dot{V}_{\pi1}$ and $\dot{V}_\beta$ are derived as follows:

$$\dot{V}_{\pi1} = -\frac{1}{\eta_1}\pi_1^T\pi_1, \tag{36}$$

$$\begin{aligned}\dot{V}_\beta =& -\frac{1}{\xi}\beta^T\beta + \beta^T\rho(\cdot) \\ \leq& -(\frac{1}{\xi} - \frac{1}{2})\beta^T\beta + \frac{1}{2}\rho^T(\cdot)\rho(\cdot).\end{aligned} \tag{37}$$

By differentiating V_{z1} and combining (19) and (28), one gets

$$\begin{aligned}\dot{V}_{z1} =& z_1^T(z_2 + \beta + \alpha_1 + K_1(x_{1f} - \hat{x}_1)) \\ \leq& -c_1 z_1^T z_1 + \frac{1}{2}\beta^T\beta + z_1^T z_2.\end{aligned} \tag{38}$$

According to (20) and (31), the time derivative of V_{z2} is obtained as follows:

$$\begin{aligned}\dot{V}_{z2} =& z_2^T(\Gamma u + \hat{W}^T S(\hat{x}) + K_2(x_{1f} - \hat{x}_1) - \dot{\omega}_2) \\ &+ z_2^T\Gamma(\tau - u) - \sum_{i=1}^n \tilde{W}_i^T\Gamma_i^{-1}\dot{\hat{W}}_i \\ =& z_2^T\Gamma(\tau - u) + z_2^T(-z_1 - c_2 z_2 - z_2) \\ &- \sum_{i=1}^n \tilde{W}_i^T(z_{2,i}S(\hat{x}) - \sigma_i\hat{W}_i).\end{aligned} \tag{39}$$

Using Young's inequality yields

$$z_2^T\Gamma(\tau - u) \leq \|z_2\|\|\Gamma\|\sqrt{n\delta_\tau^2} \leq \frac{1}{2}z_2^T z_2 + \frac{n\partial_d^2}{2}\delta_\tau^2, \tag{40}$$

$$\begin{aligned}-\sum_{i=1}^n \tilde{W}_i^T(z_{2,i}S(\hat{x}) - \sigma_i\hat{W}_i) \leq& \frac{1}{2}z_2^T z_2 + \sum_{i=1}^n \frac{\sigma_i}{2}\|W_i\|^2 \\ &- \sum_{i=1}^n \frac{\sigma_i - 1}{2}\tilde{W}_i^T\tilde{W}_i.\end{aligned} \tag{41}$$

Substituting (40) and (41) into (39), we get

$$\begin{aligned}\dot{V}_{z2} \leq & -z_1^T z_2 - c_2 z_2^T z_2 - \sum_{i=1}^{n} \frac{\sigma_i - 1}{2} \tilde{W}_i^T \tilde{W}_i \\ & + \frac{n\partial_d^2}{2}\delta_\tau^2 + \sum_{i=1}^{n} \frac{\sigma_i}{2} \|W_i\|^2. \end{aligned} \tag{42}$$

Following the common procedure of the DSC stability analysis [24,25,33], the compact set Ψ_1 is introduced to support the subsequent proof: $\Psi_1 = \{V(t) \leq U_1\} \in \mathbb{R}^{6n+nl}$ with U_1 being a positive constant. Since the set Ψ_1 is compact, $||\rho(\cdot)||$ has a maximum value ρ^*.

Further, combining (14), (36)–(38), and (42) produces

$$\begin{aligned}\dot{V} \leq & -(\lambda_{\min}(Q) - 5)\|e\|^2 - (\frac{1}{\eta_1} - 4||P||^2||K||^2)\pi_1^T \pi_1 \\ & - c_1 z_1^T z_1 - c_2 z_2^T z_2 - \sum_{i=1}^{n} (\frac{\sigma_i - 1}{2} - ||P||^2)\tilde{W}_i^T \tilde{W}_i \\ & - (\frac{1}{\xi} - 1)\beta^T \beta + \vec{\Xi} \\ \leq & -AV + \vec{\Xi}, \end{aligned} \tag{43}$$

where

$$\begin{aligned} A = & \min\Big\{ \frac{\lambda_{\min}(Q) - 5}{\lambda_{\max}(P)}, 2[(1/\eta_1) - 4||P||^2||K||^2], 2c_1, 2c_2, \\ & \frac{\sigma_i - 1 - 2||P||^2}{\lambda_{\max}(\Gamma_i^{-1})}, 2[(1/\xi) - 1] \Big\}, \\ \vec{\Xi} = & \Xi + \frac{1}{2}\rho^{*2} + \frac{n\partial_d^2}{2}\delta_\tau^2 + \sum_{i=1}^{n} \frac{\sigma_i}{2}\|W_i\|^2. \end{aligned}$$

From the inequality (43), it follows that $\dot{V}(t) < 0$ on $V(t) = U_1$ provided that $A > \vec{\Xi}/U_1$. Therefore, the set Ψ_1 is positively invariant. That is, if $V(t_x^m) \leq U_1$, then $V(t) \leq U_1$ holds for all $t \in [t_x^m, t_x^{m+1})$, indicating that the variables e_1, e_2, z_1, z_2, π_1, and $\tilde{W}_i (i = 1, \ldots, n)$ are bounded. Based on the coordinate transformation, it can be further shown that all signals remain bounded within the flow set C.

In the Jump Set D (Case 2): Due to the fact that e_1, e_2, z_1, z_2, and $\tilde{W}_i (i = 1, \ldots, n)$ stay invariant for all $t = t_{x,i}^m$, they still maintain boundedness in the set D. According to (22), (34) and (35), it follows that

$$\Delta(V_e + V_{z1} + V_{z2} + V_\beta) = 0, \tag{44}$$

$$\begin{aligned}\Delta V_{\pi 1}(t) = & V_{\pi 1}(t^+) - V_{\pi 1}(t) \\ = & \frac{1}{2}\pi_1^T(t^+)\pi_1(t^+) - \frac{1}{2}\pi_1^T(t)\pi_1(t) \\ \leqslant & -V_{\pi 1}(t) + \ell, \end{aligned} \tag{45}$$

where ℓ denotes the upper bound of $V_{\pi 1}$ in the set C.

Then, we can get

$$\Delta V(t) \leqslant -V_{\pi 1}(t) + \ell, \quad \forall t = t_{x,i}^m. \tag{46}$$

From (46), we conclude that when $V_{\pi 1}(t_{x,i}^m) > \ell$, $\Delta V(t_{x,i}^m) < 0$ holds. Therefore, provided that $V_{\pi 1}(t_{x,i}^m) > \ell$ is ensured, it follows from Lemma 1 that all signals are bounded in the jump set D. To satisfy the aforementioned prerequisite, the upper bound of $V_{\pi 1}$ in the set C should be appropriately reduced, which can be achieved by properly tuning the design parameters such as control gains and filter gains.

Next, we prove that the proposed dual ETMs do not exhibit Zeno behavior. Define $\mu_{1,i}(t) = x_{1,i}(t) - \breve{x}_{1,i}(t)$ for $t \in [t_{x,i}^m, t_{x,i}^{m+1})$, and $\wp_i(t) = u_i(t) - \tau_i(t)$ for $t \in [t_{\tau,i}^{\bar{m}}, t_{\tau,i}^{\bar{m}+1})$, whose derivatives are given by

$$\frac{d}{dt}|\mu_{1,i}(t)| = sign(x_{1,i}(t) - \breve{x}_{1,i}(t))\dot{x}_{1,i}(t) \leqslant |\dot{x}_{1,i}|, \tag{47}$$

$$\frac{d}{dt}|\wp_i(t)| = sign(u_i(t) - \tau_i(t))\dot{u}_i(t) \leqslant |\dot{u}_i|. \tag{48}$$

Since all signals of the system are bounded, there exist positive constants $\bar{\lambda}_{x,i}$ and $\bar{\lambda}_{u,i}$ such that $|\dot{x}_{1,i}| \leqslant \bar{\lambda}_{x,i}$ and $|\dot{u}_i| \leqslant \bar{\lambda}_{u,i}$ hold. Due to $\mu_{1,i}(t_{x,i}^m) = 0$ and $\wp_i(t_{\tau,i}^{\bar{m}}) = 0$, we can obtain that $t_{x,i}^{m+1} - t_{x,i}^m \geqslant \delta_{x1}/\bar{\lambda}_{x,i} > 0$ and $t_{\tau,i}^{\bar{m}+1} - t_{\tau,i}^{\bar{m}} \geqslant \delta_\tau/\bar{\lambda}_{u,i} > 0$. Thus, Zeno behavior is precluded. To sum up, the proof of Theorem 1 is completed.

4. Simulation Results

To examine the effectiveness of the proposed control method, this paper considers the following two-link RM:

$$M(q) = \begin{bmatrix} \phi_1 + 2\phi_2\cos(q_2) & \phi_3 + \phi_2\cos(q_2) \\ \phi_3 + \phi_2\cos(q_2) & \phi_4 \end{bmatrix}, \tag{49}$$

$$C(q,\dot{q}) = \begin{bmatrix} -\phi_2\sin(q_2)\dot{q}_2 & -2\phi_2\sin(q_2)\dot{q}_2 \\ \phi_2\sin(q_2)\dot{q}_1 & 0 \end{bmatrix}, \tag{50}$$

$$G(q) = \begin{bmatrix} \phi_5\cos(q_1) + \phi_6\cos(q_1+q_2) \\ \phi_6\cos(q_1+q_2) \end{bmatrix}, \tag{51}$$

where $\phi_1 = (m_1+m_2)l_1^2 + m_2l_2^2 + J_1$, $\phi_2 = m_2l_1l_2$, $\phi_3 = m_2l_2^2$, $\phi_4 = \phi_3 + J_2$, $\phi_5 = (m_1+m_2)l_1$ g, and $\phi_6 = m_2l_2$ g. For $i = 1, 2$, $m_i = m_{o,i} + \Delta m_i$, $l_i = l_{o,i} + \Delta l_i$, and $J_i = J_{o,i} + \Delta J_i$ denote the ith link masses, lengths and inertia values, respectively. $m_{o,i}$, $l_{o,i}$ and $J_{o,i}$ are the nominal values, where $m_{o,1} = 1.2$ kg, $m_{o,2} = 0.8$ kg, $l_{o,1} = 1.0$ m, $l_{o,2} = 0.7$ m, $J_{o,1} = 5.2$ kg $\cdot$ m^2 and $J_{o,2} = 5.2$ kg $\cdot$ m^2. Δm_i, Δl_i and ΔJ_i are the uncertain parameters.

To better reflect the actual situation, we introduce the following expressions for the friction and the process fault:

$$F(q,\dot{q}) = \begin{bmatrix} 0.5\dot{q}_1 + 1.2\sin(2q_1) + 0.5\cos(\dot{q}_1) \\ 0.3\dot{q}_2 + 2.4\sin(q_1) - 0.5\cos(\dot{q}_2) \end{bmatrix}, \tag{52}$$

$$\varphi(q,\dot{q}) = \begin{bmatrix} 4\sin(q_1q_2) + 8\cos(q_1\dot{q}_2) - 2 \\ 2\cos(q_1q_2) - 6\sin(\dot{q}_1\dot{q}_2) + 4 \end{bmatrix}, \tag{53}$$

$$\gamma_1(t-10) = \begin{cases} 0, & t < 10 \\ 1 - e^{-8(t-10)}, & t \geq 10 \end{cases} \tag{54}$$

$$\gamma_2(t-10) = \begin{cases} 0, & t < 10 \\ 1 - e^{-10(t-10)}. & t \geq 10 \end{cases} \tag{55}$$

The FLS employs the following set of membership functions:

$$\mu_{F_i^l}(x_i) = \exp\left(-\frac{(x_i + 5 - l)^2}{4}\right), \tag{56}$$

where $l = 1, \ldots, 9$ and $i = 1, \ldots, 4$.

The design parameters and initial conditions of the controller are listed in Table 1. The simulation results are displayed in Figures 1–8. The torque inputs under ETM are shown in Figure 1, and their amplitudes remain within a reasonable range. Figure 2 depicts the norms of the adaptive laws. Figures 3 and 4 illustrate the trajectories of the observer errors e_1 and e_2, respectively, demonstrating that the designed observer effectively estimates the joint velocity of the RM. Figures 5 and 6 show the triggering moments and intervals for the system output, while Figures 7 and 8 present those for the system input. The above results verify the effectiveness of the proposed control method.

Table 1. Design Parameters and Initial Conditions.

$x_1(0) = [0,0]^T$, $x_2(0) = [0,1]^T$, $\hat{x}_1(0) = [0.5,0.5]^T$, $\hat{x}_2(0) = [0,0]^T$,
$x_{1f}(0) = [0.2,0.2]^T$, $\omega_2(0) = [0,0]^T$, $\hat{W}_1(0) = \hat{W}_2(0) = \mathbf{0}_{9\times1}$,
$c_1 = 0.05$, $c_2 = 100$, $\eta_1 = 0.1$, $\xi = 2.5$, $r_1 = 2$, $r_2 = 2$,
$K_1 = \mathrm{diag}\{50,50\}$, $K_2 = \mathrm{diag}\{100,100\}$,
$\Gamma_1 = 50\,\mathbf{I}_{9\times9}$, $\Gamma_2 = 50\,\mathbf{I}_{9\times9}$, $\delta_{x1} = 0.4$, $\delta_\tau = 1.6$.

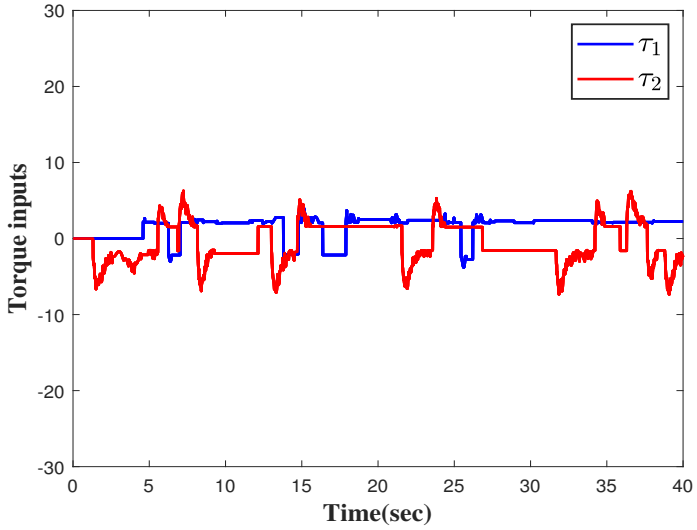

Figure 1. Torque inputs τ_1 and τ_2.

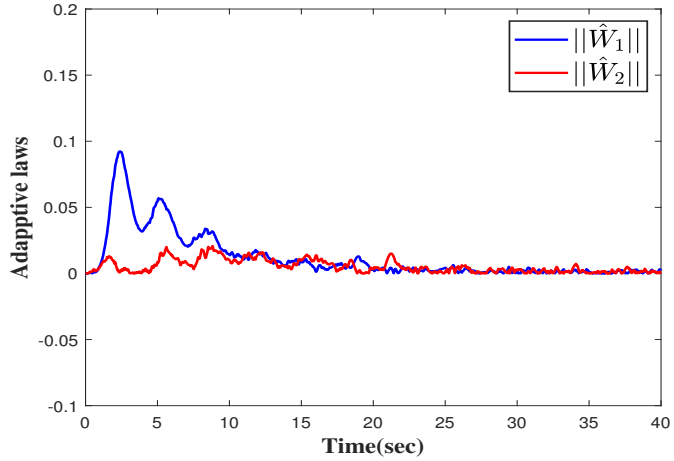

Figure 2. Norms of adaptive laws.

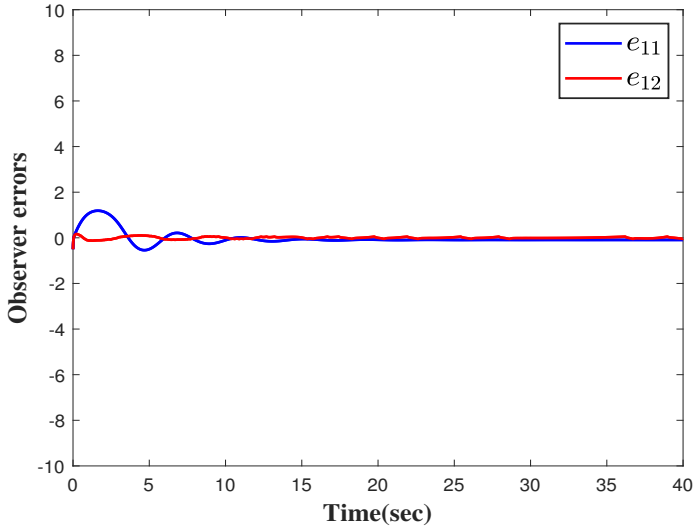

Figure 3. Observer errors e_{11} and e_{12}.

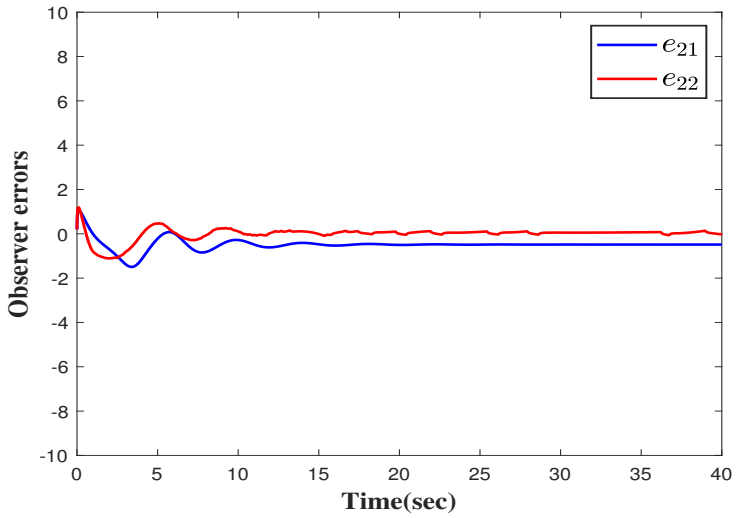

Figure 4. Observer errors e_{21} and e_{22}.

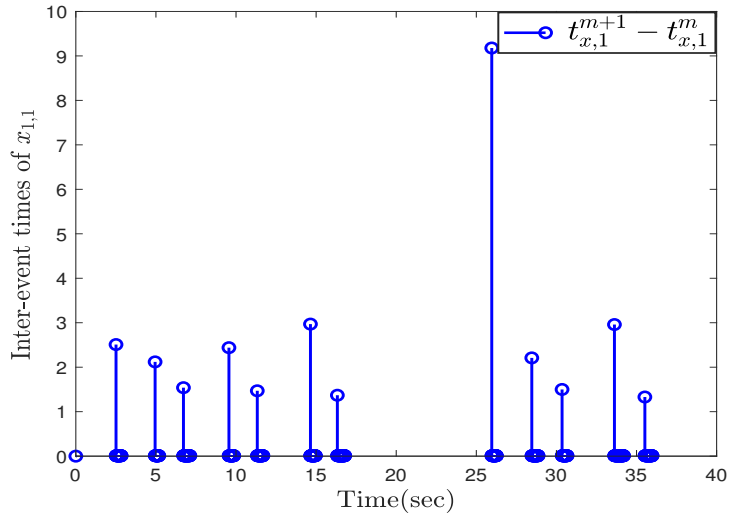

Figure 5. Interevent times of $x_{1,1}$.

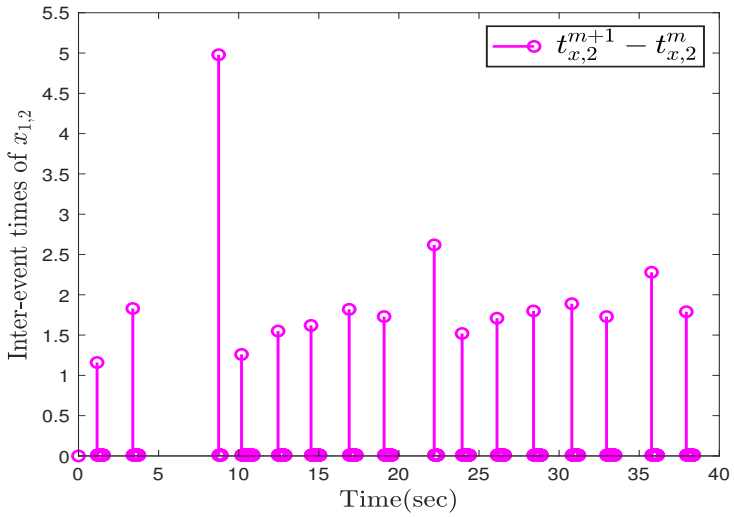

Figure 6. Interevent times of $x_{1,2}$.

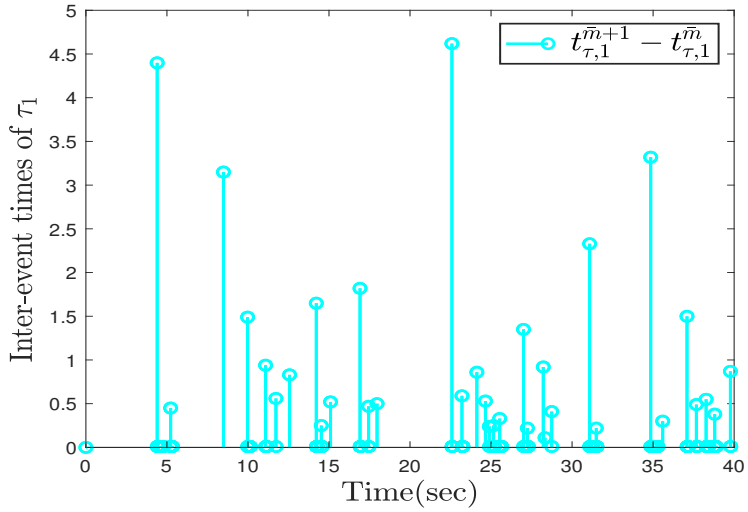

Figure 7. Interevent times of τ_1.

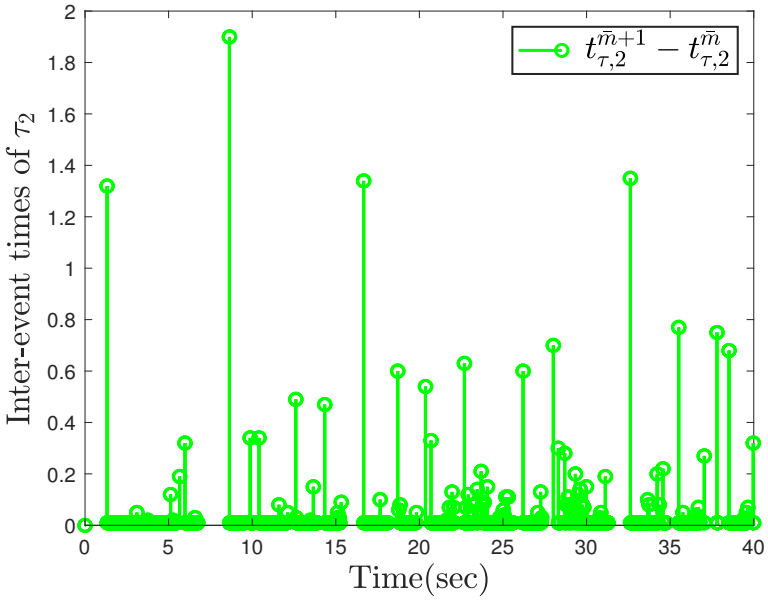

Figure 8. Interevent times of τ_2.

5. Conclusions

This paper has proposed an effective control protocol with input and output triggering for an uncertain RM. To tackle the challenge caused by the discontinuity of the sampled output, a first-order filter was designed to generate a continuously differentiable filtered version. Then, considering that the velocity signal could not be measured, a fuzzy state observer was designed, which achieved excellent state estimation without requiring the RM information. In addition, the Lyapunov stability theorem of the hybrid system was used to prove the boundedness of the system signals. Finally, the derived control protocol was verified by the two-link RM. In future work, we will further investigate the effectiveness of the proposed control method for RMs under general sensor fault models.

Author Contributions

J.S.: methodology, software, writing—original draft preparation; A.M.: visualization; B.N.: investigation, supervision; Y.M.: validation; D.K.J.: conceptualization; D.Z.: data curation. All authors have read and agreed to the published version of the manuscript.

Funding

This research was funded in part by the National Natural Science Foundation of China (Nos. U25A20455, 62376170, 62506052), in part by the in part the Natural Science Foundation of Liaoning Province of China (No.

2025-MS-013), in part by the Natural Science Foundation of Chongqing of China (No. CSTB2025NSCQ-GPX0746), in part by China Postdoctoral Science Foundation (No. 2025M771718), and in part by Postdoctoral Fellowship Program of China Postdoctoral Science Foundation (No. GZC20251189).

Data Availability Statement

Not applicable.

Conflicts of Interest

Given the role as Co Editors-in-Chief, Ben Niu had no involvement in the peer review of this paper and had no access to information regarding its peer-review process. Full responsibility for the editorial process of this paper was delegated to another editor of the journal.

Use of AI and AI-Assisted Technologies

No AI tools were utilized for this paper.

References

1. Huang, H.; Chen, Y. Evolutionary optimization of fuzzy reinforcement learning and its application to time-varying tracking control of industrial parallel robotic manipulators. *IEEE Trans. Ind. Inform.* **2023**, *19*, 11712–11720.
2. Steinhauser, A.; Swevers, J. An efficient iterative learning approach to time-optimal path tracking for industrial robots. *IEEE Trans. Ind. Inform.* **2018**, *14*, 5200–5207.
3. Nie, S.; Qian, L.; Chen, L.; et al. Barrier lyapunov functions-based dynamic surface control with tracking error constraints for ammunition manipulator electro-hydraulic system. *Def. Technol.* **2021**, *17*, 836–845.
4. Choi, B.; Lee, W.; Park, G.; et al. Development and control of a military rescue robot for casualty extraction task. *J. Field Robot.* **2019**, *36*, 656–676.
5. Cheah, C.C.; Li, X.; Yan, X.; et al. Simple pd control scheme for robotic manipulation of biological cell. *IEEE Trans. Autom. Control.* **2014**, *60*, 1427–1432.
6. Fu, J.; Burzo, I.; Iovene, E.; et al. Optimization-based variable impedance control of robotic manipulator for medical contact tasks. *IEEE Trans. Instrum. Meas.* **2024**, *73*, 1–8.
7. Wang, H.; Li, Y. Adaptive control of robot manipulators with closed architecture. *Automatica* **2024**, *162*, 111040.
8. Zhao, X.; Liu, Z.; Jiang, B.; et al. Switched controller design for robotic manipulator via neural network-based sliding mode approach. *IEEE Trans. Circuits Syst. II Express Briefs* **2022**, *70*, 561–565.
9. Harandi, M.R.J.; Hassani, A.; Hosseini, M.I.; et al. Adaptive position feedback control of parallel robots in the presence of kinematics and dynamics uncertainties. *IEEE Trans. Autom. Sci. Eng.* **2023**, *21*, 989–999.
10. Ma, H.; Ren, H.; Zhou, Q.; et al. Observer-based neural control of n-link flexible-joint robots. *IEEE Trans. Neural Netw. Learn. Syst.* **2022**, *35*, 5295–5305.
11. Qin, Q.; Gao, G.; Zhong, J. Finite-time adaptive extended state observer-based dynamic sliding mode control for hybrid robots. *IEEE Trans. Circuits Syst. II Express Briefs* **2022**, *69*, 3784–3788.
12. Rayguru, M.M.; Mohan, R.E.; Parween, R.; et al. An output feedback based robust saturated controller design for pavement sweeping self-reconfigurable robot. *IEEE/ASME Trans. Mechatron.* **2021**, *26*, 1236–1247.
13. Zhai, J.; Li, Z. Fast-exponential sliding mode control of robotic manipulator with super-twisting method. *IEEE Trans. Circuits Syst. II Express Briefs* **2021**, *69*, 489–493.
14. Sui, J.; Niu, B.; Ou, Y.; et al. Event-triggered adaptive finite-time control for a robotic manipulator system with global prescribed performance and asymptotic tracking. *IEEE Trans. Cybern.* **2025**, *55*, 1045–1055.
15. Xu, H.; Yu, D.; Sui, S.; et al. An event-triggered predefined time decentralized output feedback fuzzy adaptive control method for interconnected systems. *IEEE Trans. Fuzzy Syst.* **2022**, *31*, 631–644.
16. Xie, Y.; Ma, Q.; Wang, Z. Adaptive fuzzy event-triggered tracking control for nonstrict nonlinear systems. *IEEE Trans. Fuzzy Syst.* **2021**, *30*, 3527–3536.
17. Li, Y.; Wei, M.; Tong, S. Event-triggered adaptive neural control for fractional-order nonlinear systems based on finite-time scheme. *IEEE Trans. Cybern.* **2022**, *52*, 9481–948.
18. Cao, L.; Pan, Y.; Liang, H.; et al. Observer-based dynamic event-triggered control for multiagent systems with time-varying delay. *IEEE Trans. Cybern.* **2022**, *53*, 3376–3387.
19. Wang, X.; Zhou, Y.; Luo, B.; et al. Event-triggered neuro-adaptive fixed-time control for nonlinear switched and constrained systems: An initial condition-independent method. *IEEE Trans. Circuits Syst. I Regul. Pap.* **2023**, *71*, 2229–2239.
20. Yuan, W.; Liu, Y.-H.; Su, C.-Y.; et al. Whole-body control of an autonomous mobile manipulator using model predictive control and adaptive fuzzy technique. *IEEE Trans. Fuzzy Syst.* **2022**, *31*, 799–809.
21. Alonso, R.; Bonini, A.; Recupero, D.R.; et al. Exploiting virtual reality and the robot operating system to remote-control a humanoid robot. *Multimed. Tools Appl.* **2022**, *81*, 15565–15592.

22. Deng, Y.; Zhang, X.; Im, N.; et al. Model-based event-triggered tracking control of underactuated surface vessels with minimum learning parameters. *IEEE Trans. Neural Netw. Learn. Syst.* **2019**, *31*, 4001–4014.
23. Li, Y.; Yang, G.; Tong, S. Fuzzy adaptive distributed event-triggered consensus control of uncertain nonlinear multiagent systems. *IEEE Trans. Syst. Man Cybern. Syst.* **2018** *49*, 1777–1786.
24. Zhang, Z.; Wen, C.; Xing, L.; et al. Adaptive event-triggered control of uncertain nonlinear systems using intermittent output only. *IEEE Trans. Autom. Control.* **2021**, *67*, 4218–4225.
25. Zhang, Z.; Wen, C.; Xing, L.; et al. Event-triggered adaptive control for a class of nonlinear systems with mismatched uncertainties via intermittent and faulty output feedback. *IEEE Trans. Autom. Control.* **2023**, *68*, 8142–8149.
26. Zhang, Z.; Wen, C.; Xing, L.; et al. Adaptive output feedback control of nonlinear systems with mismatched uncertainties under input/output quantization. *IEEE Trans. Autom. Control.* **2022**, *67*, 4801–4808.
27. Zhang, Z.; Wen, C.; Zhao, K.; et al. Decentralized adaptive control of uncertain interconnected systems with triggering state signals. *Automatica* **2022**, *141*, 110283.
28. Hu, Y.; Yan, H.; Wang, M.; et al. Fuzzy observer-based input/output event-triggered control for euler–lagrange systems with guaranteed performance and input saturation. *IEEE Trans. Fuzzy Syst.* **2023**, *32*, 2077–2088.
29. Xu, S.; He, B. Robust adaptive fuzzy fault tolerant control of robot manipulators with unknown parameters. *IEEE Trans. Fuzzy Syst.* **2023**, *31*, 3081–3092.
30. Niu, B.; Sui, J.; Zhao, X.; et al. Adaptive fuzzy practical predefined-time bipartite consensus tracking control for heterogeneous nonlinear mass with actuator faults. *IEEE Trans. Fuzzy Syst.* **2024**, *32*, 3071–3083.
31. Haddad, W.M.; Chellaboina, V.; Nersesov, S.G. Impulsive and hybrid dynamical systems: stability, dissipativity, and control. In *Impulsive and Hybrid Dynamical Systems*; Princeton University Press: Princeton, NJ, USA, 2014.
32. Sahoo, A.; Xu, H.; Jagannathan, S. Neural network-based event-triggered state feedback control of nonlinear continuous-time systems. *IEEE Trans. Neural Netw. Learn. Syst.* **2015**, *27*, 497–509.
33. Sui, J.; Liu, C.; Niu, B.; et al. Prescribed performance adaptive containment control for full-state constrained nonlinear multiagent systems: A disturbance observer-based design strategy. *IEEE Trans. Autom. Sci. Eng.* **2025**, *22*, 179–190.